
This manuscript is a preprint on EarthArXiv and has been submitted for publication in Communications Earth & Environment. Please note that the manuscript has not undergone peer review, and subsequent versions may have slightly different content. The DOI of the peer-reviewed publication will be provided if accepted. Please contact any of the authors with questions or feedback.

Quantifying water availability in basins holding the majority of global lithium resources

Alexander Kirshen¹, Brendan J. Moran¹, Lee Ann Munk², Aeon Russo², Sarah McKnight^{1,3}, Jordan Jenckes^{2,4}, Daniel Corkran¹, Magdalen Bresee¹, and David Boutt¹

1. Department of Earth, Geographic, and Climate Sciences, University of Massachusetts Amherst, 627 North Pleasant Street, 233 Morrill Science Center, Amherst, 01002 MA, USA

2. Department of Geological Sciences, University of Alaska Anchorage, 3211 Providence Drive, Anchorage, 99508 AK, USA

3. Department of Geology and Environmental Geosciences, University of Dayton, 300 College Park, Dayton, 45469 OH, USA

4. Department of Chemistry, University of Alaska Anchorage, 3211 Providence Drive, Anchorage, 99508 AK, USA

Corresponding author: Alexander Kirshen (akirshen@umass.edu)

Abstract

Demand for lithium is expected to increase by as much as 40 times over the coming decades. More than half the world's lithium resources are found in brine aquifers at the intersection of Chile, Argentina, and Bolivia. As lithium exploration increases, accurate estimates of water availability are critical for water management decisions, particularly in this region home to communities and ecosystems relying on limited water resources. We develop the first region-specific water availability assessment with 28 active, near-production, and prospective lithium-producing basins. We modify the AWARE method by re-calculating availability minus demand using a novel available water approach and evaluate the impacts of freshwater use from future lithium mining. Our results reveal that commonly used hydrologic models overestimate streamflow by as much as 6000%, leading to inaccurate water scarcity classifications. We also find that, on average, water availability could decrease by 8-107% depending on lithium production quantity and processing technology.

Introduction

The renewable energy transition is one of the most important challenges human civilization faces¹. As green technology continues to advance, batteries for electronic devices, electric cars, and electrical grids are critical². Lithium is a key component in modern batteries, and demand for this critical mineral is projected to increase by as much as 40 times over the coming decades^{3,4}. Fifty-three percent of the world's resources of lithium are found in highly saline aquifers (or brines) where evaporation has exceeded precipitation for millions of years, creating elevated concentrations of solutes including lithium⁵⁻⁹. These deposits form in closed (endorheic) basins and are preferentially located in a region of South America referred to as the Lithium Triangle¹⁰.

The Lithium Triangle is located in the Dry Andes of South America at the intersection of Bolivia, Chile, and Argentina (Figure 1). Elevations are high and variable (2300 - 6800 meters above sea level) with large spatial climate variability. This region is semi-arid to hyper-arid with mean annual precipitation ranging from ~20 mm in the west to ~250 mm in the east^{11,12}. Precipitation is event-driven with little to none in the winter and larger events in the summer. The hydrologic system is complex with intermittent streams largely sourced by groundwater storage, and lagoons with large seasonal fluctuations sustained by both modern precipitation and groundwater storage^{13,14}. Precipitation, groundwater discharge, and streamflow are critical for sustaining diverse ecosystems ranging from microbial lagoon communities to larger fauna^{15,16}. Human populations are generally small, but many communities in the region rely on fresh groundwater and surface water resources¹⁷.

A growing body of research is investigating the influence of lithium brine mining activities on local communities, ecosystems, and water scarcity^{4,13,17-22}. Though no significant direct impacts from lithium brine extraction on freshwater resources or salar wetlands have been shown to date, the risks will increase with continued development, especially considering ongoing uncertainties regarding hydrology in these regions^{13,16}. With growing concerns over environmental and societal impacts, battery manufacturers will need to further consider the sustainability of their lithium sources. Accurate estimates of water availability are imperative²³, as they are often a key input into lithium-related life cycle assessments (LCA) and are used for water management decisions^{20,21,24}. This will become ever more important as the impacts of global climate change in this region become more pronounced. These impacts include rising temperatures, increasing length and severity of droughts, and the frequency and intensity of anomalous precipitation events^{13,17}.

Watershed-scale water scarcity and availability are often assessed with global hydrologic models^{1,25-28}. Global hydrologic models provide informative water demand, groundwater, and river discharge data²⁹⁻³². However, these models are limited in spatial scale³³ and often produce inaccurate river discharge estimates due to assumptions behind precipitation forcings, streamflow generation, and gaps in calibration data^{29,30}. In arid regions, traditional hydrologic models often overestimate river discharge^{32,34,35}. To date no studies have assessed the accuracy of river discharge estimates from global hydrologic models or quantitatively evaluated available water specifically for basins within the Lithium Triangle.

To characterize water scarcity, we utilize the Available Water REMaining (AWARE) method²⁵. AWARE is a LCA midpoint indicator used to assess water scarcity and quantifies the amount of water remaining in a watershed after demands for humans and ecosystems have been met²⁵. In this study, we use calculations of availability minus demand (AMD) and characterization factors (AWARE CF) adopted from Boulay et al.²⁵. The data provided in this study can be applied to other LCA methods to understand water scarcity, like the commonly used water scarcity index (ratio of water demand to availability).

The two processing technologies that produce lithium carbonate (a final lithium product for batteries) from brine are evaporative technology and direct lithium extraction (DLE). Both these methods consume brine and freshwater⁴. The evaporative method consists of pumping brine from aquifers into evaporation ponds where over 90% of water volume is lost to solar evaporation, increasing lithium concentrations to ~6000 ppm. The concentrated solution is then sent to a processing plant to remove impurities and Li_2CO_3 is precipitated^{4,20,36}. In contrast, most DLE processes use limited or no solar evaporation and encompass several different sub-methods. The general steps of DLE are pumping brine, pre-processing (e.g., heating or pH adjustment), the site-specific DLE process, and post-processing, although some techniques do require evaporation ponds as an initial step⁴. Of the eight full-scale lithium brine operations as of 2022, seven use 100% evaporative technology while only one (Salar del Hombre Muerto) uses DLE⁴. Freshwater use per tonne of lithium carbonate equivalent (FW/LCE) varies between evaporative technologies and DLE. Vera et al.⁴ compiled FW/LCE data from scientific articles and reports of several DLE variations. They found that out of the reports that included freshwater use, 33% consumed less, 11% consumed similar, 25% consumed more, and 31% consumed over 10 times more freshwater than evaporation ponds.

Our study aims to address the following questions for this region: 1) What is the most accurate long-term average precipitation product to use as an input for available water calculations, 2) How can we accurately quantify available water, and 3) How do increases in freshwater consumption from Li mining impact water availability?

To that end, we developed the Lithium Closed Basin Water Availability (LiCBWA) method. This is the first basin-scale region-specific water availability assessment encompassing 12 active or near-production and 16 prospective lithium-producing basins (Figure 1). We modify the AWARE²⁵ method by re-calculating AMD with a novel available water approach (defined as groundwater recharge plus streamflow) while maintaining a similar method of calculating demand (human water consumption from WaterGAP 2.2^{37,38} plus environmental flow requirements). The lower and upper bounds on available water are defined by three groundwater recharge representations and a range of precipitation-to-streamflow coefficients based on streamflow field measurements of all the significant streams within the Salar de Atacama, Salar del Hombre Muerto, and Salar de Pastos Grandes watersheds. The LiCBWA approach is relevant to all endorheic basins, although this specific model is calibrated with data from the Lithium Triangle.

To identify the precipitation product with the most reliable long-term average representation of the region's precipitation, we compared mean annual precipitation from 10 global datasets with observations from 26 meteorological stations. Following recent research assessing the large and

diverse array of global precipitation products available^{39,40}, we chose a subset of products to analyze which cover gauge-based, satellite-related, and precipitation reanalysis methods. Due to specific strengths, weaknesses, and biases inherent in each of these methods, the resulting precipitation estimates for any given site can vary widely. We believe this group of datasets provides a robust assessment of the variability and diversity in precipitation available with which to determine a suitable precipitation dataset. Our approach is unique as we use Argentinian meteorological stations which largely stopped recording data in the 1990's⁴¹ (green triangles within Argentina, Figure 1). These stations are not used for calibration in global products although they provide valuable comparison points within the Lithium Triangle. While it is common for studies to assess precipitation products at monthly intervals, we chose to assess precipitation with long-term averages (11- and 21-year intervals) because the goal of the assessment was to have the most accurate input precipitation datasets for long-term average available water. The two periods of record used to assess precipitation products were 1980-1990 and 1996-2016. The analysis presented here should not be used to inform monthly or annual precipitation product accuracy.

We compare stream discharge results from two hydrologic models - WaterGAP 2.2 (WaterGAP)^{37,38} and PCR-GLOBWB 2.0 (PCR-GLOBWB)⁴². WaterGAP and PCR-GLOBWB are the input models for widely used water scarcity and availability products like the National Geographic and Utrecht University Water Gap, Aqueduct Water Risk Atlas, World Wildlife Fund Water Risk Filter, and AWARE²⁵⁻²⁸. These products are also used to assess current global water security and projected future streamflow in the Sixth Assessment Report from the Intergovernmental Panel on Climate Change^{1,43,44}.

We then quantify how freshwater consumption related to lithium mining reduces water availability when producing 10, 20, and 70 thousand tonnes LCE using evaporative technologies and DLE. To calculate freshwater use for evaporative technologies, we use the average of two FW/LCE values from operations at the Salar de Atacama and Salar de Olaroz-Cauchari (36 m³/tonne), and for DLE we use 71 m³/tonne based on the only full-scale DLE operation⁴. Annual LCE production targets of 10, 20, 70 thousand tonnes are used because these values represent the range of production targets for Argentinian basins in this study⁴⁵.

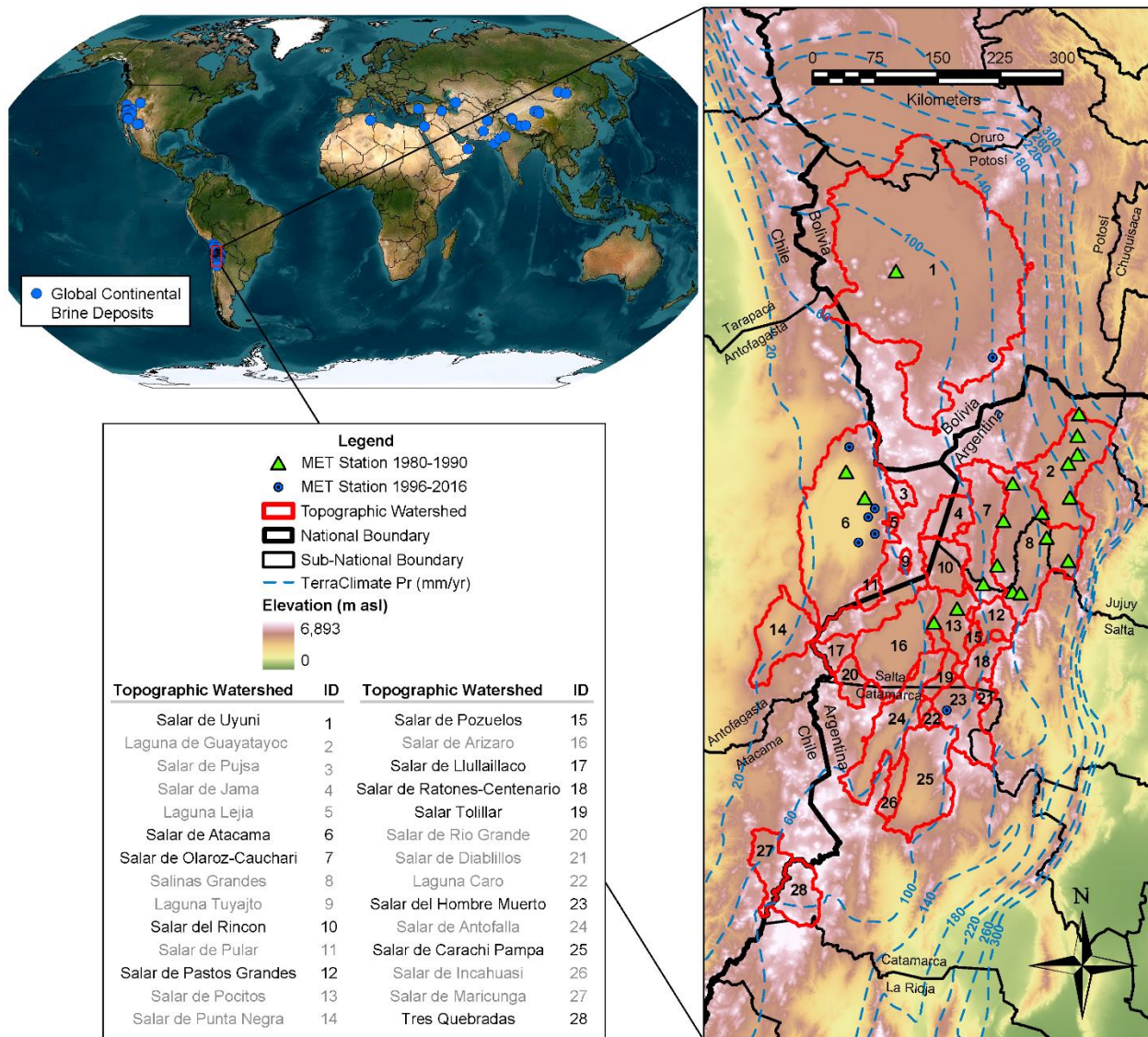


Figure 1: World map showing the spatial distribution of global lithium continental brine deposits. The study region in the inset map shows topographic watersheds in red, national boundaries with thick black lines, and sub-national boundaries with thin black lines. Basin names and IDs are included in the lower left table with black text representing active or near-production lithium operations and gray text representing a prospective site. The dotted blue lines represent mean annual precipitation contours from TerraClimate (1958-2022). The shaded background represents elevation in meters above sea level from the ALOS World 3D DEM. The meteorological stations used to assess precipitation in the region are shown as green triangles or blue dots depending on their period of record.

Results

Precipitation Assessment

TerraClimate produces the most accurate long-term average precipitation for this region with the lowest mean absolute error (MAE) and root-mean-square error (RMSE) (Figure 2d and Table S1). Nine of the 10 precipitation products assessed (all but TerraClimate) overestimate precipitation by at least 100% at more than a third of the meteorological stations, while 7 of the products overestimate precipitation by at least 200% at more than a third of the stations. Generally among all 10 products, the basins with the largest percent difference (>100%) between climate model and weather station precipitation are Salar de Atacama, Salar del Hombre Muerto, and Salar de Olaroz-Cauchari, while the basins with the smallest percent difference (<100%) are in Salar de Uyuni and Laguna de Guayatayoc. We included map panels showing the spatial distribution of annual precipitation difference (mm) of the three input precipitation products to LiCBWA (Figure 2a), WaterGAP (Figure 2b), and PCR-GLOBWB (Figure 3c). WFDEI and CRU overestimate precipitation at 81% (21 sites) and 88% (23 sites), respectively, while TerraClimate is more balanced with 42% of stations overestimating (11 sites). WFDEI and CRU overestimate by at least 100 mm/year in the eastern stations, while TerraClimate underestimates by at least 100 mm/year in the northeast of the study area (Laguna Guayatayoc). For all products, the absolute difference between climate model and weather station precipitation increases as elevation increases (Figure S1). When only using the stations with at least a 95% complete record, TerraClimate continues to have the lowest MAE and RMSE (Table S1). We also analyzed TRMM, GPM IMERG, and CMORPH CDR, but these products do not have historical records that extend back to 1980 (Figure S2 and Table S1).

Basin-Scale Available Water and Demand

Geographic and quantitative results of average available water (groundwater recharge plus streamflow), water demand (human water consumption from WaterGAP plus environmental flow requirements), and average AMD are shown in Figure 3 and Table S2. Available water, water demand, and AMD all generally increase moving east, following trends in precipitation (Figure S3). Average precipitation ranges from 20 to 205 mm/year with coefficients of variation ranging from 0.16 to 0.66 (Figure S3). Available water is the key driver of AMD; although water demand and available water are both largest in the same basins, AMD follows the same spatial trend as available water. Average AMD values among all basins range from 1 to 18 mm/year with an average of 6 mm/year (Figure 3c), a stark contrast to the world average annual AMD from Boulay et al.²⁵ of ~160 mm. Streamflow (R) contributes on average 81% of total available water, with a range of 64 to 91% (Figure 3a). Demand is dominated by environmental water requirements and contributes on average 95% of water demand, with a range of 63 to 100% (Figure 3b).

Comparison with WaterGAP 2.2 and PCR-GLOBWB 2.0

LiCBWA provides the most accurate streamflow estimates with a MAE of 3 mm/year (26%) (Figure 4a). WaterGAP and PCR-GLOBWB have MAE of 168 mm/year (1322%) and 482 mm/year (3800%), respectively (Figure 4a). When comparing available water from LiCBWA with WaterGAP and PCR-GLOBWB (Figure 4b) available water from WaterGAP is greater than LiCBWA in 61% of basins, while PCR-GLOBWB is greater in 96% of basins. On average, WaterGAP and PCR-GLOBWB estimate available water to be 75 and 219 mm/year greater than LiCBWA estimates. The median available water (excluding outliers) of all 28 basins from

LiCBWA is 10 mm/year, while the median available water from WaterGAP and PCR-GLOBWB are 55 and 165 mm/year (Figure 4c).

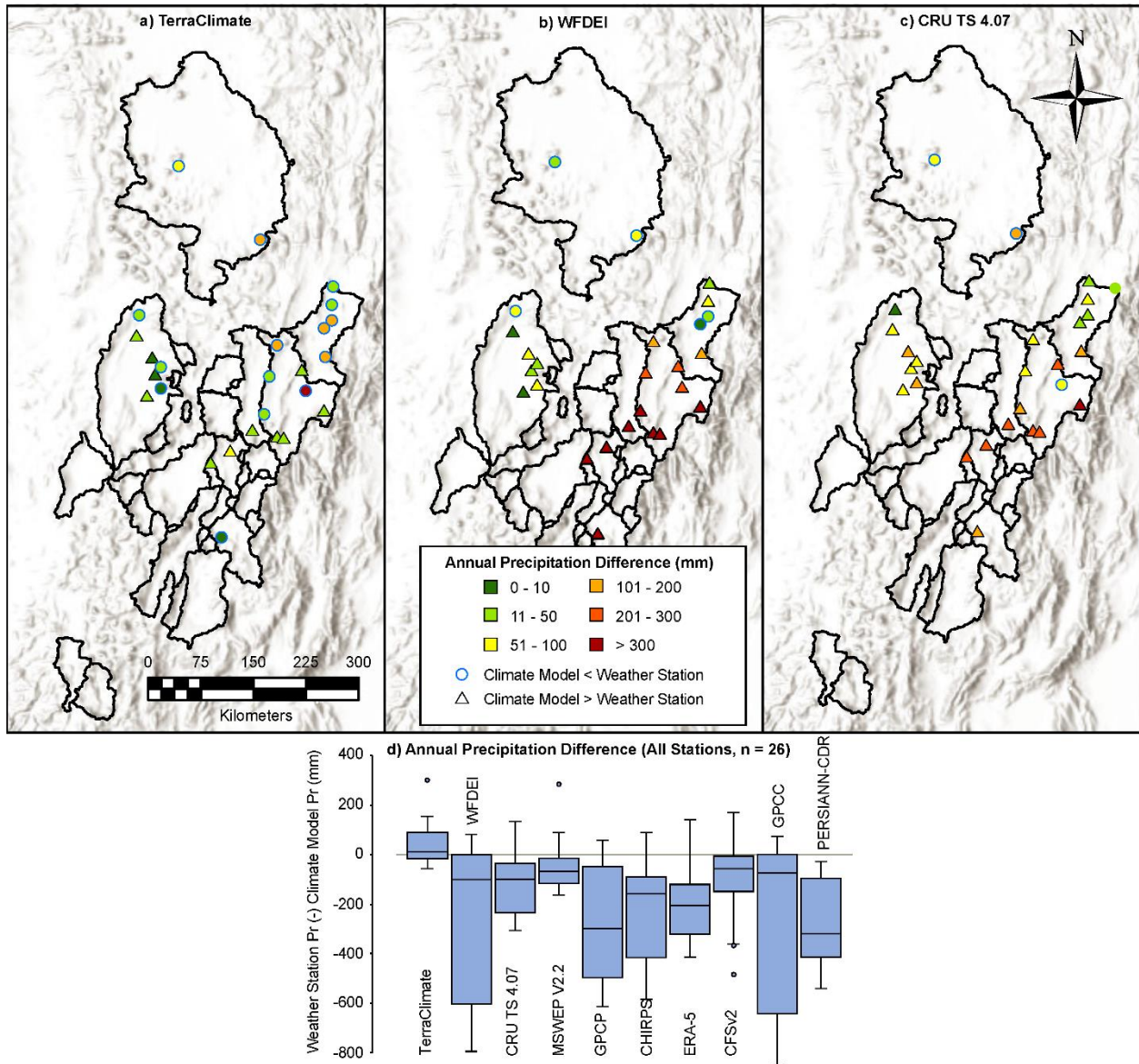


Figure 2: Panels a, b, and c show annual precipitation differences between each meteorological station and the corresponding global precipitation datasets used for this study (LiCBWA), WaterGAP, and PCR-GLOBWB – TerraClimate (a), WFDEI (b), and CRU TS 4.07 (c), respectively. The color of the symbol represents the difference in precipitation. If the climate model precipitation is greater than the corresponding weather station data, the symbol is a triangle, and if the model is less than the corresponding weather station data, the symbol is a circle. Box plots of annual precipitation differences for all the global precipitation datasets assessed are included in (d). The box is bounded by the IQR, and the outliers are greater than 1.5 x the IQR.

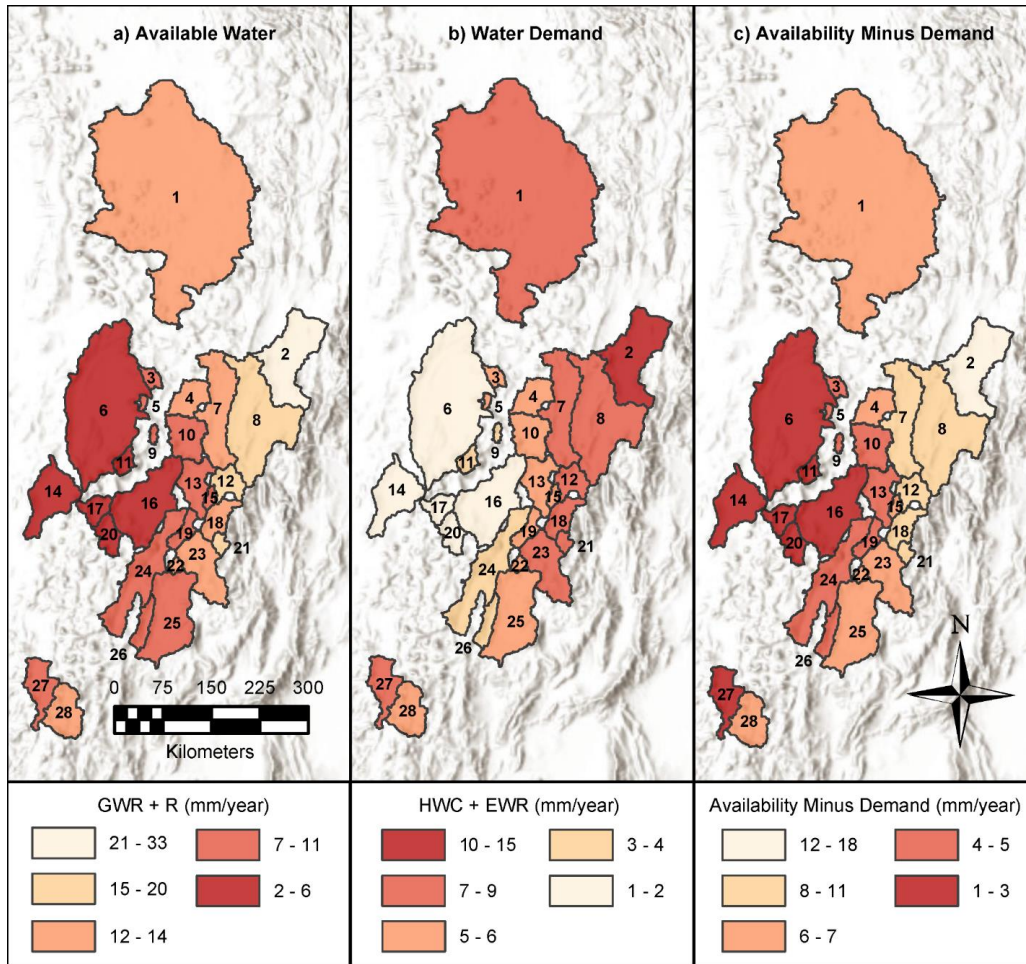


Figure 3: Results of available water, water demand, and availability minus demand calculations from this study. a) Average available water calculated as groundwater recharge (GWR) plus streamflow (R). b) Water demand calculated as human water consumption from WaterGAP (HWC) plus environmental water requirements (EWR). c) Average availability minus demand is calculated as available water minus demand.

The AWARE CF varies when using average AMD calculations from the LiCBWA, WaterGAP, and PCR-GLOBWB methods which impacts the water scarcity classification of most basins. LiCBWA classifies more basins as critical (27) compared to WaterGAP (13) and PCR-GLOBWB (1) (Figure 4d). Of the basins where we have measured streamflow and greater confidence in AMD and AWARE CF (Salar de Atacama, Salar de Pastos Grandes, and Salar del Hombre Muerto), LiCBWA classifies all three as critical, WaterGAP classifies Salar de Atacama as critical, and PCR-GLOBWB classifies all three as uncritical. When using measured streamflow for these basins, they are all classified as critically water scarce.

Impact of Lithium Mining Water Use

Current full-scale direct lithium extraction will reduce availability minus demand by double when compared to evaporative technologies (Figure 5). For example, the average AMD

reduction when producing 20 kilo-tonnes per annum (ktpa) LCE is 31% for DLE and 16% for evaporative technology. The variation in AMD reduction is largely controlled by basin size; the four smallest basins (with watershed areas less than 400 km²) have the largest percent change in AMD, while the largest basin has the smallest reduction (Figure 5). AMD reduction is also impacted by variations in groundwater recharge and streamflow fluxes. For example, the Salar de Atacama is the second largest basin, but has the sixth smallest AMD reduction due to the relatively low available water input (4 mm/year).

Each basin has uncertainty regarding freshwater impacts from lithium mining due to each basin's range of AMD estimates (Table S2). When assuming the low-end AMD for each basin, 3, 8, and 16 basins will have no water remaining (AMD_{Li} values less than 0) when incorporating freshwater use from DLE and producing 10, 20, and 70 ktpa LCE, respectively (Table S3). When using the upper-end AMD values, 9 basins will have no water remaining when producing 70 ktpa using DLE, but when producing 10 and 20 ktpa, all basins have water remaining. When assuming the low-end AMD calculation and freshwater use from evaporative technology, 2, 3, and 13 basins will have no water remaining with 10, 20, and 70 ktpa LCE, respectively; with the upper-end AMD, 2 basins will have no water remaining when producing 70 ktpa, but all basins will have water remaining with the two other producing targets (Table S3).

To understand how availability minus demand decreases could impact hydrologic systems in the Lithium Triangle, we can use insights from Corkran et al.⁴⁶. They developed two-dimensional groundwater flow and transport models of the inflow zones of the Salar de Atacama and the Salar del Hombre Muerto to understand the relationship between freshwater and brine pumping and groundwater discharge to wetlands. In these models, they simulated the freshwater pumping flux as 40% of groundwater inflow, which is comparable to an ~80% reduction in AMD (Figure S4). Corkran et al.⁴⁶ found that the simulated total flux to wetlands decreased by 26-34% with freshwater pumping, and remotely sensed vegetated areas decreased significantly. Although this does not directly quantify how freshwater use from lithium mining will impact all of these basins, it provides valuable insight into possible consequences of decreasing water availability.

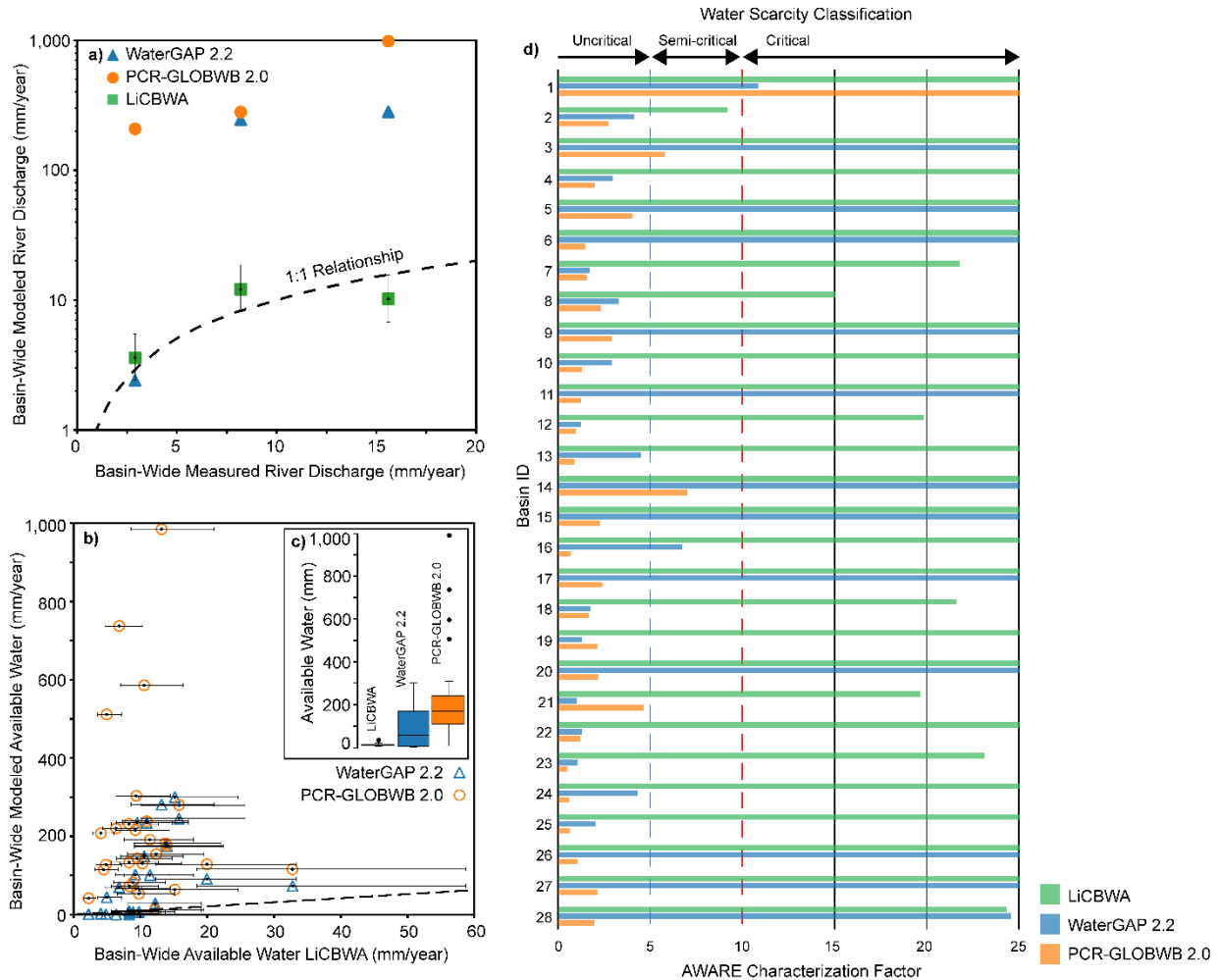


Figure 4: a) Basin-wide average modeled river discharge vs. basin-wide river discharge from field measurements (3 total) for WaterGAP (blue triangle), PCR-GLOBWB (orange circle), and this study (LiCBWA, green square). Upper and lower bounds are included for LiCBWA and represent the minimum and maximum streamflow calculations. b) Basin-wide modeled available water from WaterGAP (blue triangle) and PCR-GLOBWB (orange circle) vs. basin-wide average modeled available water from LiCBWA for all 28 basins. Upper and lower bounds are defined from ranges in groundwater recharge and streamflow. c) Box plots of average available water for all three models. The box is bounded by the IQR, and the outliers are greater than 1.5 x the IQR. d) Water scarcity classifications based on average AMD. The bottom axis shows AWARE characterization factors calculated from WaterGAP (blue), PCR-GLOBWB (orange) and LiCBWA. The top axis shows water scarcity classifications from Schomberg et al. (2021), with CF cutoffs represented as blue and red dotted lines.

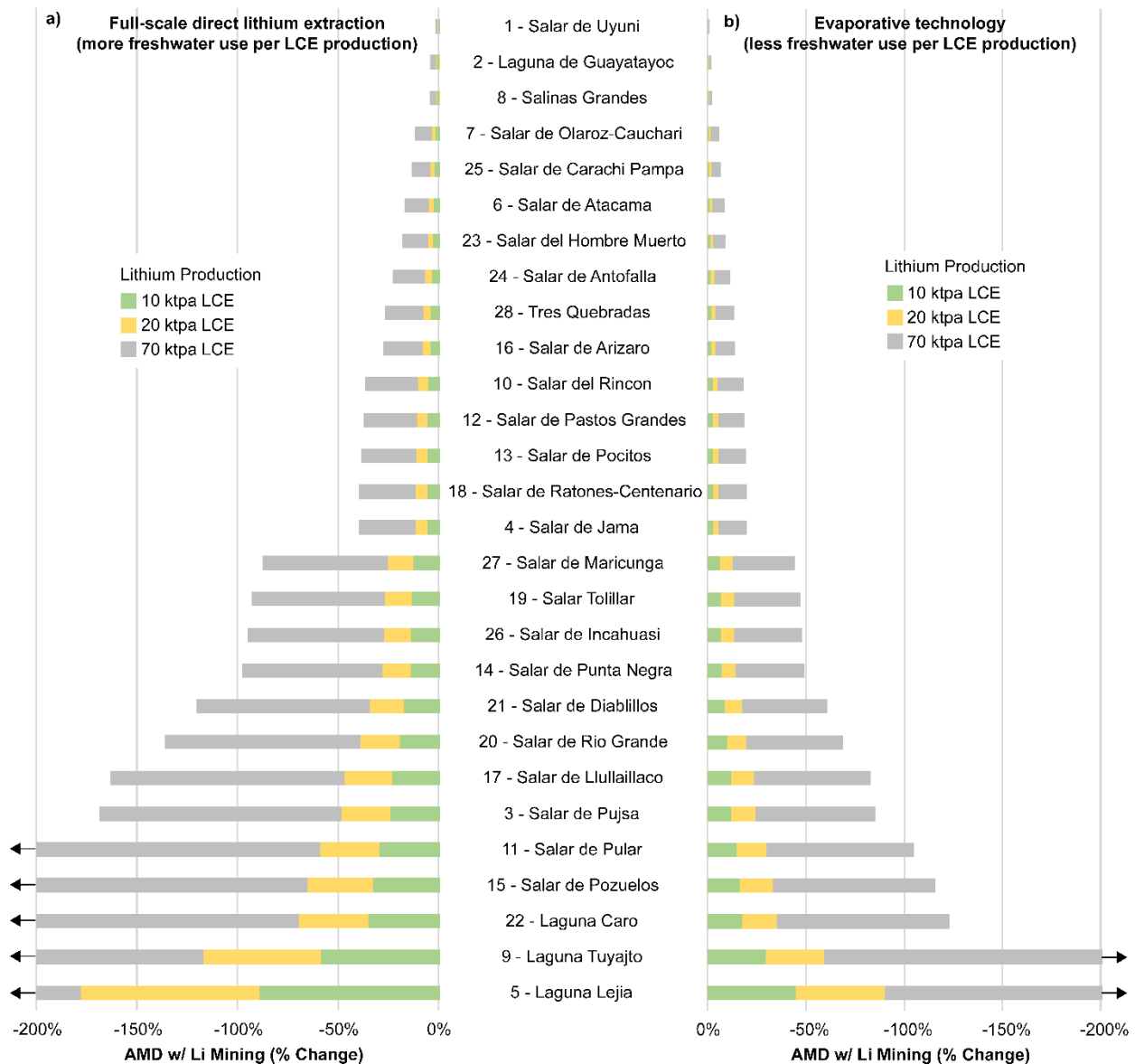


Figure 5: Percent change in average availability minus demand when incorporating water use from lithium mining. The colors within each bar represent AMD decreases associated with different annual production of lithium carbonate equivalent (LCE) in kilo-tonnes per annum (ktpa). Panel a) shows AMD reductions when using the only current full-scale DLE technology, and panel b) shows AMD reductions when using current full-scale evaporative technology.

Discussion

Simplified and Improved Water Budget Conceptualization

We provide a new water budget conceptualization unique to arid, endorheic basins of the Dry Andes. Global hydrologic models can be complex with multiple water compartments (e.g.,

canopy, snow, soil, surface water, groundwater) and include meteorological forcings where surface water and groundwater storage are calculated on a cell-by-cell basis^{29,33}. Because this region consists of only endorheic basins, we assume that each watershed is a closed hydrologic system where all modern groundwater recharge and streamflow is sourced from precipitation and storage within basin boundaries, and water demand will impact available water only in the corresponding basin. With this assumption, we can simplify the approach by calculating long-term average groundwater recharge and streamflow using region-specific equations and methods. We indirectly model evapotranspiration through our available water approach instead of using actual evapotranspiration products which can have large uncertainties^{32,47}.

Our study improves the current understanding of how much water is naturally available in the Lithium Triangle. This is also the first study to assess the accuracy of two commonly used global hydrologic models specifically for this region. Based on measured streamflow data, our available water results (LiCBWA) are more accurate than WaterGAP and PCR-GLOBWB. In general, WaterGAP and PCR-GLOBWB overestimate streamflow, which is connected to an overestimation of precipitation. For example, in the Salar de Atacama modeled precipitation is overestimated by 20 mm/year for WaterGAP (WFDEI) and by 94 mm/year for PCR-GLOBWB (modeled output⁴²) (based on 7 meteorological stations within the basin polygon). Corresponding simulated river discharge is within 1 mm/year for WaterGAP and overestimated by 205 mm/year for PCR-GLOBWB. In the Salar del Hombre Muerto precipitation is overestimated by a staggering 570 mm/year for WaterGAP and 191 mm/year for PCR-GLOBWB (based on 1 meteorological station within the basin polygon). Corresponding simulated river discharge is overestimated by 270 mm/year for WaterGAP and 970 mm/year for PCR-GLOBWB. The positive correlation between streamflow and precipitation has been previously shown for both models, as well as for other global water models³². The other likely source of overestimation is the specific method of simulating streamflow generation. On average 19% of precipitation becomes streamflow (range of 0 to 43%) in the WaterGAP model, and 101% of precipitation becomes streamflow (range of 9 to 321%) in PCR-GLOBWB. The upper end of these ranges are unrealistic in endorheic basins, particularly when streamflow is greater than precipitation (>100%)^{48,49}. The LiCBWA approach estimates that 12% of precipitation becomes average available water (streamflow plus groundwater recharge) with a range of 9 to 16%.

Uncertainty remains in the groundwater recharge and streamflow estimates associated with the complex hydrologic dynamics of these basins and the climate and streamflow monitoring network across the study region. Some streamflow and groundwater may be sourced from long flow paths from adjacent basins. In addition, some inflow may be from long recharge pathways and groundwater storage releases that represent wetter climates of the past^{13,14}. Accurate streamflow measurements are limited to three basins in the region. Although these three basins represent a relatively large range of elevation, annual precipitation, and area, they may not be representative of all the basins analyzed. Additionally, the meteorological stations used here have limited coverage in the south of the Lithium Triangle and between 2700 to 3200 meters above sea level (Figure S1).

To continue improving our quantification of water availability, the hydrologic, geochemical, and meteorological monitoring network must be expanded. Measuring monthly streamflow in additional basins will improve our understanding of streamflow generation. Seasonal

geochemical water sampling of fresh groundwater, transitional groundwater, streamflow, and lagoons will help define the sources and ages of water to continue improving how we define available water in the Lithium Triangle. Installing meteorological stations in all active and potential lithium-producing basins with a large range of elevations will allow for continued improvement of precipitation products.

Implications for Water Resource Management

Lithium mining requires water⁴, therefore it is important to determine how much water is available in this data sparse region. With accurate water availability quantities, we can understand how lithium mining will impact water scarcity (AMD) and the greater hydrologic system. With our improved understanding of water availability, we find that all but one of the basins in the study is classified as critically water scarce without incorporating current or future water use from mining. When incorporating this mining water use, AMD will decrease on average 15-107% with the current DLE technology, and 8-54% with evaporative technology. Decreases in AMD of ~80% have been shown to reduce discharge to wetlands and reduce vegetated areas, although reductions in wetland discharge and AMD do not necessarily scale linearly⁴⁶. This provides a low-end estimate of wetland impacts with the assumption that freshwater pumping is equally spatially distributed along inflow zones; this may not be accurate in some operations, as pumping can be concentrated in sub-basins leading to potentially greater impacts over a smaller area.

We do not attempt to provide specific allowable water use rates, as this would require further basin-specific analysis. However, we do find that smaller basins (<1400 km²) could have double the reduction in AMD when compared to larger basins. The two exceptions to this are the Salar de Punta Negra and Salar de Maricunga; this can be explained by the extremely low input precipitation to Salar de Punta Negra (lowest of any basin) and relatively large HWC at Salar de Maricunga (highest HWC to AW ratio of any basin). With these findings, freshwater allocations must be considered at a basin to sub-basin scale. In the past, freshwater has not been properly allocated within the largest lithium brine producing basin in the world¹³. In addition, we show that different mining technologies and production targets can have a large impact on water availability, and these factors must be a priority when planning and evaluating the water sustainability of a lithium brine project. Because lithium mining is a reality in the Lithium Triangle, scientists, local communities, and producers must collaborate to reduce freshwater use and monitor precipitation, streamflow, and groundwater levels to improve the understanding of each water system while maintaining the health of ecosystems.

Methods

Defining Basins

We delineated the 28 active or prospective lithium-producing topographic watersheds using the HydroSheds product⁵⁰. To meet the requirements of a lithium-producing basin, each basin needed to have a clearly defined basin floor with a salar nucleus (25 basins) or saline lake (3 basins). We defined active or near-production as currently producing lithium products (lithium

hydroxide, lithium carbonate, lithium chloride) or 1-3 years until full-scale production. Basin floor elevations are from the ALOS World 3D DEM.

Precipitation Assessment

Meteorological precipitation data were collected from the National Meteorological and Hydrological Service of Bolivia (Senamhi), the Center for Climate and Resilience Research Climate Explorer, and the National Agricultural Technology Institute of Argentina (INTA) (see ‘Data Availability’ section). Because the dates of record vary among the meteorological stations, two periods of average annual precipitation from 1980-1990 (19 sites) and 1996-2016 (7 sites) were selected to maximize the spatial and temporal distribution of observation sites. Nineteen stations have >95% complete records, while the other 7 have >73% record. We compared station data with 13 global precipitation datasets⁵¹⁻⁶³. For nine of the precipitation products, we calculated average annual precipitation from both 1980-1990 and 1996-2016 for all 26 stations. For PERSIANN-CDR, average annual precipitation was calculated from 1983-1990 and 1996-2016 because the record only extends back to 1983. Only the 1996-2016 stations (7 sites) were used for GPM IMERG (2001-2016), TRMM (1998-2016), and CMORPH CDR (1998-2016) because the historical records do not extend further (Table S1). Average annual precipitation was extracted from the gridded precipitation datasets at the point location for each meteorological station for the corresponding period of record. The accuracy of the precipitation datasets was assessed using mean absolute error and root-mean-square error between the average annual precipitation of the meteorological station data and the gridded precipitation datasets.

Availability Minus Demand

We modified the AWARE method from Boulay et al.²⁵ to define availability minus demand, or AMD, which includes available water (AW), human water consumption (HWC), and environmental water requirements (EWR):

$$AMD \left(\frac{mm}{year} \right) = \frac{AW - HWC - EWR}{Watershed Area}$$

We developed a new approach to calculating available water, where available water equals groundwater recharge (GWR) plus streamflow (R):

$$AW \left(\frac{mm^3}{year} \right) = GWR + R$$

We provided a range of GWR estimates by integrating three methods: 1) Extracting mean annual recharge estimates (1968-2018) from Berghuijs et al.⁶⁴ within each basin polygon, 2) multiplying TerraClimate mean annual precipitation (1968-2018) by recharge fractions from Berghuijs et al.⁶⁴ and extracting within each basin polygon, and 3) extracting TerraClimate mean annual precipitation within each basin polygon and multiplying by a groundwater recharge power law function derived from the Salar de Atacama, where P is precipitation in mm/year⁴⁹:

$$GWR_{method\ 3} \left(\frac{mm^3}{year} \right) = (1.3 \times 10^{-4}) \times P^{2.3} \times Watershed\ Area$$

For GWR methods 2 and 3, the TerraClimate datasets were modified with the Pixel Editor Imagery tool in ArcGIS Pro within basins 13, 16, 23, and 25 because the white salar nucleus was interpreted as cloud coverage, so precipitation was overestimated on the basin floor.

Streamflow was calculated using the following equations, where C is the streamflow coefficient, $P_{RCH\ Zone}$ is TerraClimate precipitation in mm/year within the recharge zone, and $Area_{RCH\ Zone}$ is the area of the recharge zone in mm^2 . The recharge zone is defined as the watershed area minus the basin floor area (see Table S2).

$$R \left(\frac{mm^3}{year} \right) = (C \times P_{RCH\ Zone} \times Area_{RCH\ Zone})$$

The streamflow coefficient (C) is shown in the following equation, where $R_{RCH\ Zone}$ is basin-wide streamflow ($mm^3/year$) from field measurements in three basins – Salar de Atacama, Salar de Pastos Grandes, and Salar del Hombre Muerto.

$$C = \left(\frac{R_{RCH\ Zone}}{Area_{RCH\ Zone}} \right) / P_{RCH\ Zone}$$

These measurements were collected during several field campaigns between 2019-2023 using an OTT MF pro-Water Flow Meter and a USGS TopSet Wading Rod. These data were supplemented where necessary with measurements collected by the Dirección General de Aguas and environmental consultants to lithium mines. These three basins represent a relatively wide range of elevations and geographic coverage. Streamflow was calculated using the recharge zone because the vast majority of streamflow in these systems exists outside the basin floor. We use the average (0.11), minimum (0.07), and maximum (0.16) of C from the three basins to define streamflow bounds. The lower bound of AW was calculated as minimum GWR plus minimum R, and the upper bound of AW was calculated as maximum GWR plus maximum R. Average AW was calculated as the average of the three GWR methods plus average R. The average and upper and lower bounds of AMD were calculated using the AW values discussed in the previous sentence.

We used methods from Boulay et al.²⁵ to quantify HWC and EWR. Human water consumption from WaterGAP^{37,38} was downloaded from the WULCA AWARE website (see ‘Data Availability’ section). First, the data was normalized by grid area and resampled from 0.5° resolution to 0.02° resolution. Then the average consumption was extracted within each basin polygon and multiplied by the area of the basin polygon. Environmental water requirements were calculated as 0.45 multiplied by average AW. We assumed intermediate flow because we used annual averages of streamflow^{25,65}. We included GWR as part of the EWR calculation because groundwater plays a key role in supporting wetlands and ecosystems in these environments.

Comparison with WaterGAP 2.2 and PCR-GLOBWB 2.0

We extracted mean annual simulated river discharge from the WaterGAP (1960-2010) and PCR-GLOBWB (1958-2015) to compare with measured streamflow and results from this study. Actual mean monthly river availability data from WaterGAP was from the WULCA AWARE website and PCR-GLOBWB data was extracted from the Utrecht University Yoda data portal (see ‘Data Availability’ section). Both datasets were normalized by grid area and resampled to 0.02° before extracting mean annual discharge from each basin polygon. Extracted values were then multiplied by basin area. In addition, we extracted monthly precipitation from the Utrecht University Yoda data portal to calculate the percent of precipitation that becomes streamflow (see ‘Discussion’).

Characterization factors (CF) were calculated using the following equation²⁵. The CFs for this study was calculated using mean AMD. $AMD_{world\ avg}$ is 163 mm/year (or 0.0136 m/month):

$$CF = \frac{1}{\left(\frac{AMD}{AMD_{world\ avg}}\right)}$$

For WaterGAP and PCR-GLOBWB, we defined AW as river discharge. This was a conservative approach to define an upper bound on the CF. If GWR was included, CF values would decrease, and these products would further underestimate water scarcity. EWR was the product of 0.45 and river discharge, and HWC values are the same used in this study for consistency. Water scarcity was classified for each basin using CF cutoff values from Schomberg et al.²¹.

Boulay et al.²⁵ calculated AMD and CF at monthly timesteps, while our approach (LiCBWA) was calculated using long-term averages. If we calculated AMD at monthly time steps, differences could arise in CF and EWR values; the original AWARE method calculated EWR based on low, intermediate, and high flows. We assumed that average annual flows are intermediate. These factors do not influence findings from the study because we re-calculated AMD and CF for WaterGAP and PCR-GLOBWB using long-term averages of streamflow.

We also re-calculated CF from WaterGAP instead of extracting values from already calculated CF from Boulay et al.²⁵ because Boulay et al.²⁵ had gaps in spatial coverage in the study region; when extracting CF values directly from Boulay et al.²⁵, 9 basins are considered critical, 7 are semi-critical, 3 are uncritical, and 9 have more than half of basin area with no data.

Lithium Mining Impacts

We used freshwater use per LCE (FW/LCE) production values from Vera et al.⁴ to calculate the flux of freshwater used for various LCE production targets (HWC_{Li}). The FW/LCE value for evaporative technology was 36 m³/tonne, which was the average consumption of operations at

the Salar de Atacama and the Salar de Olaroz. The only full-scale active DLE operation was at the Salar del Hombre Muerto and consumed 71 m³/tonne of freshwater⁴. We then calculated AMD when incorporating 10, 20, and 70 thousand tonnes of LCE production to each basin (AMD_{Li}). We used these annual LCE values because they represented the range of production targets for Argentinian basins in this study⁴⁵. AMD percent change (Figure 5) was calculated using average AMD from ‘Availability Minus Demand’ methods section as the initial value and AMD_{Li} as the final value. AMD_{Li} was also calculated using minimum and maximum AMD values (Table S3).

$$AMD_{Li} = AMD - \left(\frac{HWC_{Li}}{Watershed\ Area} \right)$$

Data availability

Meteorological station data was extracted from the following locations: National Meteorological and Hydrological Service of Bolivia (<http://senamhi.gob.bo/index.php/onsc>), Center for Climate and Resilience Research Climate Explorer (<https://explorador.cr2.cl/>), and the National Agricultural Technology Institute of Argentina (INTA; Bianchi and Yañez, 1992). Precipitation data was downloaded from the following locations: TerraClimate (https://developers.google.com/earth-engine/datasets/catalog/IDAHO_EPSCOR_TERRACLIMATE), WFDEI (<ftp://rfddata:forceDATA@ftp.iiasa.ac.at>), CRU TS 4.07 (<https://crudata.uea.ac.uk/cru/data/hrg/>), GPCP (<https://www.ncei.noaa.gov/data/global-precipitation-climatology-project-gpcp-monthly/>), GPCC (<https://climatedataguide.ucar.edu/climate-data/gpcc-global-precipitation-climatology-centre>), CHIRPS (<https://climatedataguide.ucar.edu/climate-data/gpcc-global-precipitation-climatology-centre>), PERSIANN-CDR (<https://chrsdata.eng.uci.edu/>), MSWEP V2.2 (<https://www.gloh2o.org/mswep/>), ERA-5 (<https://cds.climate.copernicus.eu/cdsapp#!/search?type=dataset>), CMORPH CDR (<https://www.ncei.noaa.gov/data/cmorph-high-resolution-global-precipitation-estimates/access/daily/0.25deg/>), GPM IMERG L3 V06 (<https://search.earthdata.nasa.gov/search>), TRMM 3B43 V7 (<https://catalog.data.gov/dataset/trmm-tmpa-3b43-rainfall-estimate-l3-1-month-0-25-degree-x-0-25-degree-v7-trmm-3b43-at-ges->), CFSV2 (https://developers.google.com/earth-engine/datasets/catalog/NOAA_CFSV2_FOR6H). Groundwater recharge and groundwater recharge fractions from Berghuijs et al. (2022) were downloaded from (<https://zenodo.org/records/7611675>). Human water consumption (‘TOT_CU’) and river discharge from WaterGAP 2.2 were downloaded from (<https://wulca-waterlca.org/aware/input-data-watergap/>), and river discharge (‘discharge_monthAvg’) and precipitation (‘precipitation_monthTot’) from PCR-GLOBWB 2.0 was from (https://geo.data.uu.nl/research-pcrglobwb/pcr-globwb_gmd_paper_sutanudjaja_et_al_2018/).

Author Contributions

A.K., B.M., D.B, and L.M. designed the research; A.K., A.R., J.J., and M.B. collected and processed the data; A.K. analyzed the data and developed the figures; A.K. drafted the manuscript; all authors reviewed and revised the manuscript.

Competing Interests

The authors declare no competing interests.

References

1. IPCC. *Climate Change 2023: Synthesis Report. Contribution of Working Groups I, II and III to the Sixth Assessment Report of the Intergovernmental Panel on Climate Change [Core Writing Team, H. Lee and J. Romero (Eds.)]. IPCC, Geneva, Switzerland, Pp. 35-115, Doi: 10.59327/IPCC/AR6-9789291691647.* (2023).
2. Trahey, L. *et al.* Energy storage emerging: A perspective from the Joint Center for Energy Storage Research. *Proceedings of the National Academy of Sciences* **117**, 12550–12557 (2020).
3. Haddad, A. Z. *et al.* How to make lithium extraction cleaner, faster and cheaper—in six steps. *Nature* **616**, 245–248 (2023).
4. Vera, M. L., Torres, W. R., Galli, C. I., Chagnes, A. & Flexer, V. Environmental impact of direct lithium extraction from brines. *Nat Rev Earth Environ* **4**, 149–165 (2023).
5. U.S. Geological Survey. *Mineral Commodity Summaries 2023: U.S. Geological Survey.* <https://doi.org/10.3133/mcs2023> (2023).
6. Munk, L. A., Boutt, D. F., Hynek, S. A. & Moran, B. J. Hydrogeochemical fluxes and processes contributing to the formation of lithium-enriched brines in a hyper-arid continental basin. *Chem Geol* **493**, 37–57 (2018).
7. Corenthal, L. G., Boutt, D. F., Hynek, S. A. & Munk, L. A. Regional groundwater flow and accumulation of a massive evaporite deposit at the margin of the Chilean Altiplano. *Geophys Res Lett* **43**, 8017–8025 (2016).
8. Eugster, H. P. Geochemistry of evaporitic lacustrine deposits. *Annu Rev Earth Planet Sci* **8**, 35–63 (1980).
9. Rosen, M. R. The importance of groundwater in playas: a review of playa classifications and the sedimentology and hydrology of playas. (1994).
10. Munk, L. A. *et al.* Lithium brines: A global perspective. (2016).
11. Strecker, M. R. *et al.* Tectonics and climate of the southern central Andes. *Annu. Rev. Earth Planet. Sci.* **35**, 747–787 (2007).

12. Bookhagen, B. & Strecker, M. R. Orographic barriers, high-resolution TRMM rainfall, and relief variations along the eastern Andes. *Geophys Res Lett* **35**, (2008).
13. Moran, B. J. *et al.* Relic groundwater and prolonged drought confound interpretations of water sustainability and lithium extraction in arid lands. *Earths Future* **10**, e2021EF002555 (2022).
14. Moran, B. J., Boutt, D. F., Munk, L. A. & Fisher, J. D. Contemporary and Relic Waters Strongly Decoupled in Arid Alpine Environments. *PLOS Water* (2024).
15. Farias, M. E. *et al.* Prokaryotic diversity and biogeochemical characteristics of benthic microbial ecosystems at La Brava, a hypersaline lake at Salar de Atacama, Chile. *PLoS One* **12**, e0186867 (2017).
16. Frau, D. *et al.* Hydroclimatological patterns and limnological characteristics of unique wetland systems on the Argentine high Andean Plateau. *Hydrology* **8**, 164 (2021).
17. Marconi, P., Arengo, F. & Clark, A. The arid Andean plateau waterscapes and the lithium triangle: flamingos as flagships for conservation of high-altitude wetlands under pressure from mining development. *Wetl Ecol Manag* **30**, 827–852 (2022).
18. Kelly, J. C., Wang, M., Dai, Q. & Winjobi, O. Energy, greenhouse gas, and water life cycle analysis of lithium carbonate and lithium hydroxide monohydrate from brine and ore resources and their use in lithium ion battery cathodes and lithium ion batteries. *Resour Conserv Recycl* **174**, 105762 (2021).
19. Pell, R. *et al.* Towards sustainable extraction of technology materials through integrated approaches. *Nat Rev Earth Environ* **2**, 665–679 (2021).
20. Schenker, V., Oberschelp, C. & Pfister, S. Regionalized life cycle assessment of present and future lithium production for Li-ion batteries. *Resour Conserv Recycl* **187**, 106611 (2022).
21. Schomberg, A. C., Bringezu, S. & Flörke, M. Extended life cycle assessment reveals the spatially-explicit water scarcity footprint of a lithium-ion battery storage. *Commun Earth Environ* **2**, (2021).
22. Stamp, A., Lang, D. J. & Wäger, P. A. Environmental impacts of a transition toward e-mobility: the present and future role of lithium carbonate production. *J Clean Prod* **23**, 104–112 (2012).
23. Rodell, M. *et al.* Emerging trends in global freshwater availability. *Nature* **557**, 651–659 (2018).
24. Chordia, M., Wickerts, S., Nordelöf, A. & Arvidsson, R. Life cycle environmental impacts of current and future battery-grade lithium supply from brine and spodumene. *Resour Conserv Recycl* **187**, 106634 (2022).

25. Boulay, A. M. *et al.* The WULCA consensus characterization model for water scarcity footprints: assessing impacts of water consumption based on available water remaining (AWARE). *International Journal of Life Cycle Assessment* **23**, 368–378 (2018).
26. Droppers, B., Wanders, N., Bierkens, M. & Leijnse, M. World Water Map. worldwatermap.nationalgeographic.org (2023).
27. Kuzma, S. *et al.* Aqueduct 4.0: Updated Decision-Relevant Global Water Risk Indicators. *World Resources Institute* (2023) doi:10.46830/writn.23.00061.
28. WWF Water Risk Filter. riskfilter.org/water/explore/map (2021).
29. Bierkens, M. F. P. Global hydrology 2015: State, trends, and directions. *Water Resour Res* **51**, 4923–4947 (2015).
30. Sood, A. & Smakhtin, V. Global hydrological models: a review. *Hydrological Sciences Journal* **60**, 549–565 (2015).
31. Wada, Y. *et al.* Human–water interface in hydrological modelling: current status and future directions. *Hydrol Earth Syst Sci* **21**, 4169–4193 (2017).
32. Gnann, S. *et al.* Functional relationships reveal differences in the water cycle representation of global water models. *Nature Water* 1–12 (2023).
33. Telteu, C.-E. *et al.* Understanding each other’s models: an introduction and a standard representation of 16 global water models to support intercomparison, improvement, and communication. *Geosci Model Dev* **14**, 3843–3878 (2021).
34. Haddeland, I. *et al.* Multimodel estimate of the global terrestrial water balance: setup and first results. *J Hydrometeorol* **12**, 869–884 (2011).
35. Trambauer, P., Maskey, S., Winsemius, H., Werner, M. & Uhlenbrook, S. A review of continental scale hydrological models and their suitability for drought forecasting in (sub-Saharan) Africa. *Physics and Chemistry of the Earth, Parts A/B/C* **66**, 16–26 (2013).
36. Khalil, A., Mohammed, S., Hashaikeh, R. & Hilal, N. Lithium recovery from brine: Recent developments and challenges. *Desalination* **528**, 115611 (2022).
37. Flörke, M. *et al.* Domestic and industrial water uses of the past 60 years as a mirror of socio-economic development: A global simulation study. *Global Environmental Change* **23**, 144–156 (2013).
38. Müller Schmied, H. *et al.* Sensitivity of simulated global-scale freshwater fluxes and storages to input data, hydrological model structure, human water use and calibration. *Hydrol Earth Syst Sci* **18**, 3511–3538 (2014).
39. Dubey, S., Gupta, H., Goyal, M. K. & Joshi, N. Evaluation of precipitation datasets available on Google earth engine over India. *International Journal of Climatology* **41**, 4844–4863 (2021).

40. Sun, Q. *et al.* A review of global precipitation data sets: Data sources, estimation, and intercomparisons. *Reviews of Geophysics* **56**, 79–107 (2018).
41. Bianchi, A. R. & Yañez, C. Las precipitaciones en el Noroeste Argentino. *INTA. Salta* (1992).
42. Sutanudjaja, E. H. *et al.* PCR-GLOBWB 2: a 5 arcmin global hydrological and water resources model. *Geosci Model Dev* **11**, 2429–2453 (2018).
43. Gain, A. K., Giupponi, C. & Wada, Y. Measuring global water security towards sustainable development goals. *Environmental Research Letters* **11**, 124015 (2016).
44. Schewe, J. *et al.* Multimodel assessment of water scarcity under climate change. *Proceedings of the National Academy of Sciences* **111**, 3245–3250 (2014).
45. Ministerio de Economía Argentina. *Portfolio of Advanced Projects Lithium*. <https://www.argentina.gob.ar/economia/mineria/prospectors-developers-association-canada-pdac-2023/portfolio-mining-projects-2023> (2023).
46. Corkran, D. *et al.* Data for ‘Density constrains environmental impacts of fluid abstraction in continental lithium brines’. (2024) doi:<https://doi.org/10.7275/59ea-yz09>.
47. Kampf, S. K. & Tyler, S. W. Spatial characterization of land surface energy fluxes and uncertainty estimation at the Salar de Atacama, Northern Chile. *Adv Water Resour* **29**, 336–354 (2006).
48. Liu, Y., Wagener, T., Beck, H. E. & Hartmann, A. What is the hydrologically effective area of a catchment? *Environmental Research Letters* **15**, 104024 (2020).
49. Boutt, D. F., Corenthal, L. G., Moran, B. J., Munk, L. A. & Hynek, S. A. Imbalance in the modern hydrologic budget of topographic catchments along the western slope of the Andes (21–25°S): implications for groundwater recharge assessment. *Hydrogeol J* **29**, 985–1007 (2021).
50. Lehner, B., Verdin, K. & Jarvis, A. New global hydrography derived from spaceborne elevation data. *Eos, Transactions American Geophysical Union* **89**, 93–94 (2008).
51. Schneider, U. *et al.* GPCP’s new land surface precipitation climatology based on quality-controlled in situ data and its role in quantifying the global water cycle. *Theor Appl Climatol* **115**, 15–40 (2014).
52. Funk, C. *et al.* The climate hazards infrared precipitation with stations—a new environmental record for monitoring extremes. *Sci Data* **2**, 1–21 (2015).
53. Adler, R. F. *et al.* The Global Precipitation Climatology Project (GPCP) monthly analysis (new version 2.3) and a review of 2017 global precipitation. *Atmosphere (Basel)* **9**, 138 (2018).
54. Saha, S. *et al.* The NCEP climate forecast system version 2. *J Clim* **27**, 2185–2208 (2014).

55. Beck, H. E. *et al.* MSWEP V2 global 3-hourly 0.1 precipitation: methodology and quantitative assessment. *Bull Am Meteorol Soc* **100**, 473–500 (2019).
56. Hersbach, H. *et al.* The ERA5 global reanalysis. *Quarterly Journal of the Royal Meteorological Society* **146**, 1999–2049 (2020).
57. Ashouri, H. *et al.* PERSIANN-CDR: Daily precipitation climate data record from multisatellite observations for hydrological and climate studies. *Bull Am Meteorol Soc* **96**, 69–83 (2015).
58. Huffman, G. J. *et al.* The TRMM multisatellite precipitation analysis (TMPA): Quasi-global, multiyear, combined-sensor precipitation estimates at fine scales. *J Hydrometeorol* **8**, 38–55 (2007).
59. Huffman, G. J. *et al.* NASA global precipitation measurement (GPM) integrated multi-satellite retrievals for GPM (IMERG). *Algorithm theoretical basis document (ATBD) version 4*, 30 (2015).
60. Xie, P. *et al.* Reprocessed, bias-corrected CMORPH global high-resolution precipitation estimates from 1998. *J Hydrometeorol* **18**, 1617–1641 (2017).
61. Harris, I., Osborn, T. J., Jones, P. & Lister, D. Version 4 of the CRU TS monthly high-resolution gridded multivariate climate dataset. *Sci Data* **7**, 109 (2020).
62. Abatzoglou, J. T., Dobrowski, S. Z., Parks, S. A. & Hegewisch, K. C. TerraClimate, a high-resolution global dataset of monthly climate and climatic water balance from 1958–2015. *Sci Data* **5**, 1–12 (2018).
63. Weedon, G. P. *et al.* The WFDEI meteorological forcing data set: WATCH Forcing Data methodology applied to ERA-Interim reanalysis data. *Water Resour Res* **50**, 7505–7514 (2014).
64. Berghuijs, W. R., Luijendijk, E., Moeck, C., van der Velde, Y. & Allen, S. T. Global Recharge Data Set Indicates Strengthened Groundwater Connection to Surface Fluxes. *Geophys Res Lett* **49**, (2022).
65. Pastor, A. V., Ludwig, F., Biemans, H., Hoff, H. & Kabat, P. Accounting for environmental flow requirements in global water assessments. *Hydrol Earth Syst Sci* **18**, 5041–5059 (2014).

Supplemental Material

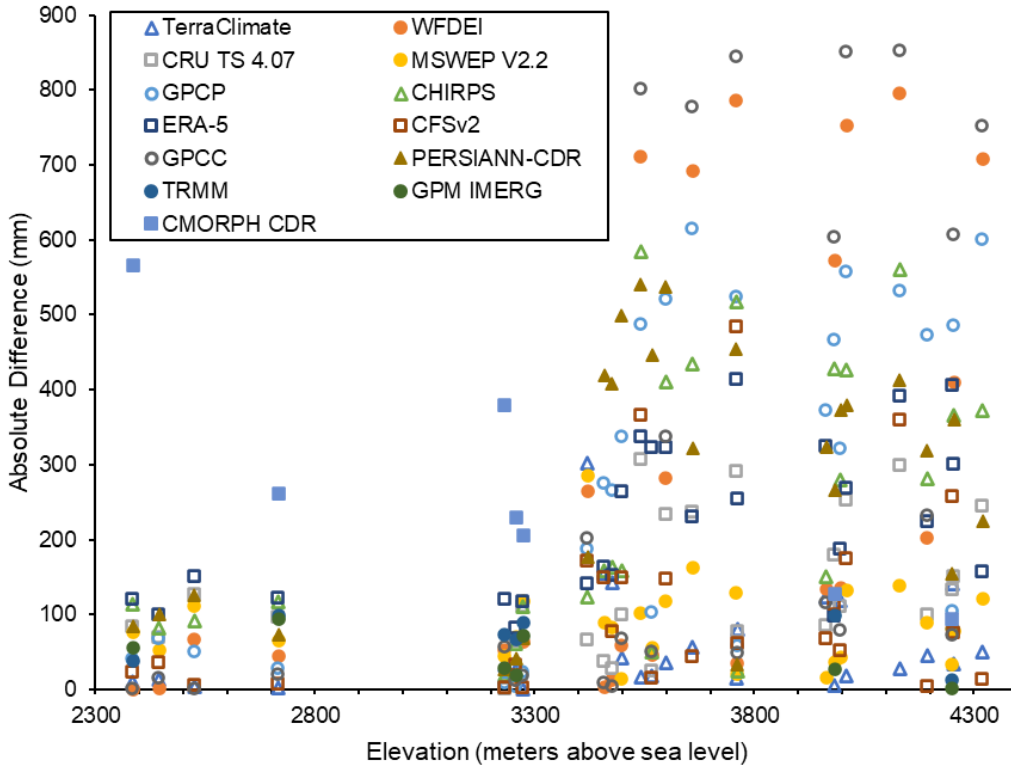


Figure S1: Absolute difference between meteorological station and gridded product mean annual precipitation for each product in mm.

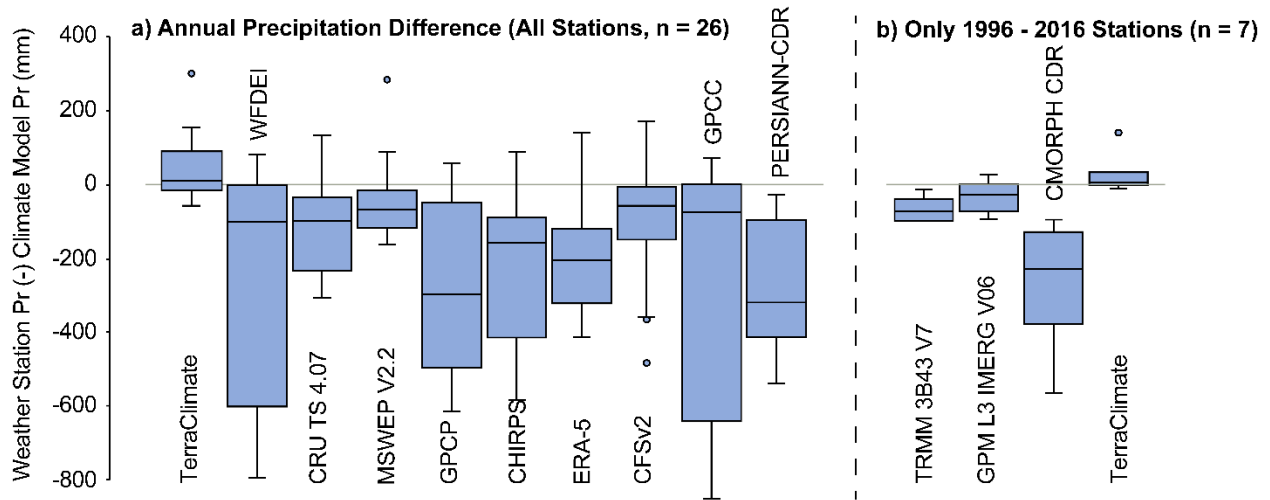


Figure S2: Box plots of the annual precipitation difference (mm) between meteorological and gridded product precipitation for all 13 products including the three that only have historical data back to ~2000.

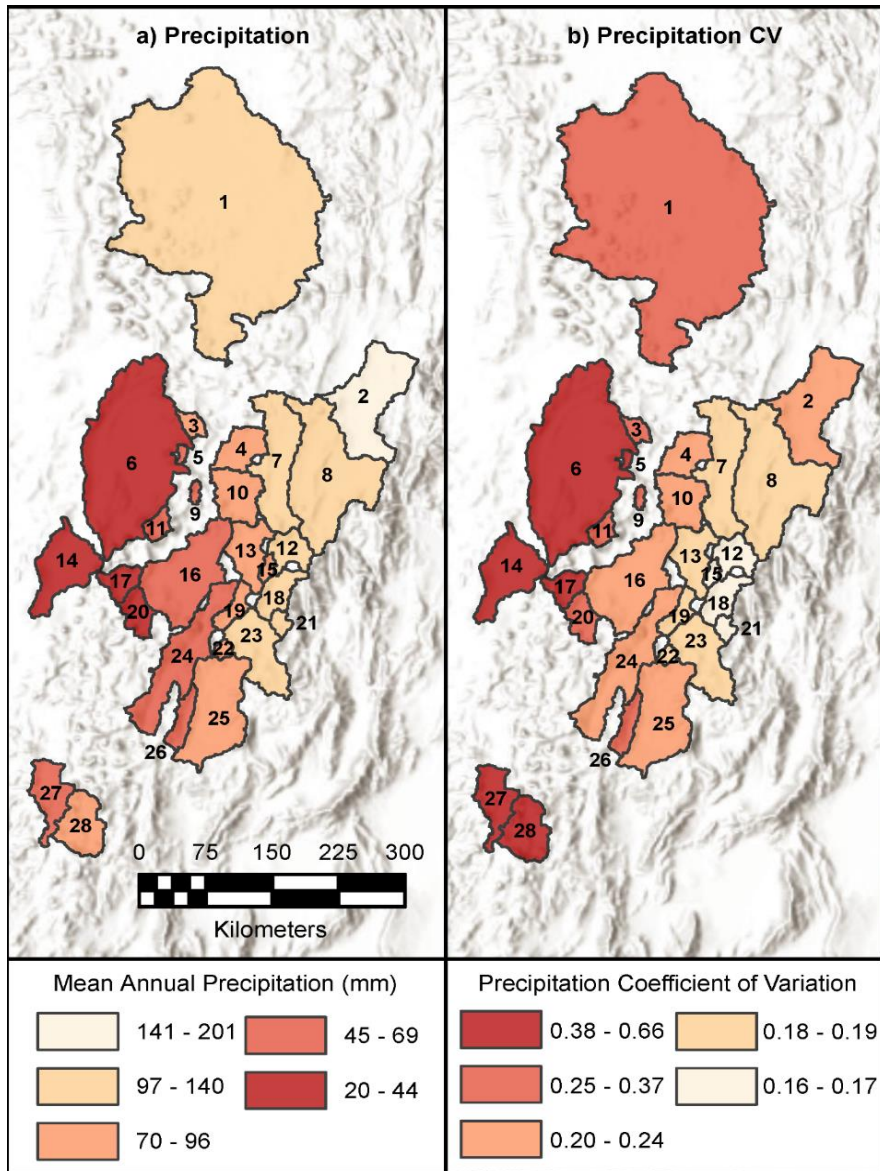


Figure S3: a) Mean annual precipitation from each basin from TerraClimate (1958-2022). b) Precipitation coefficient of variation calculated as the standard deviation of annual precipitation (1958-2022) divided by mean annual precipitation.

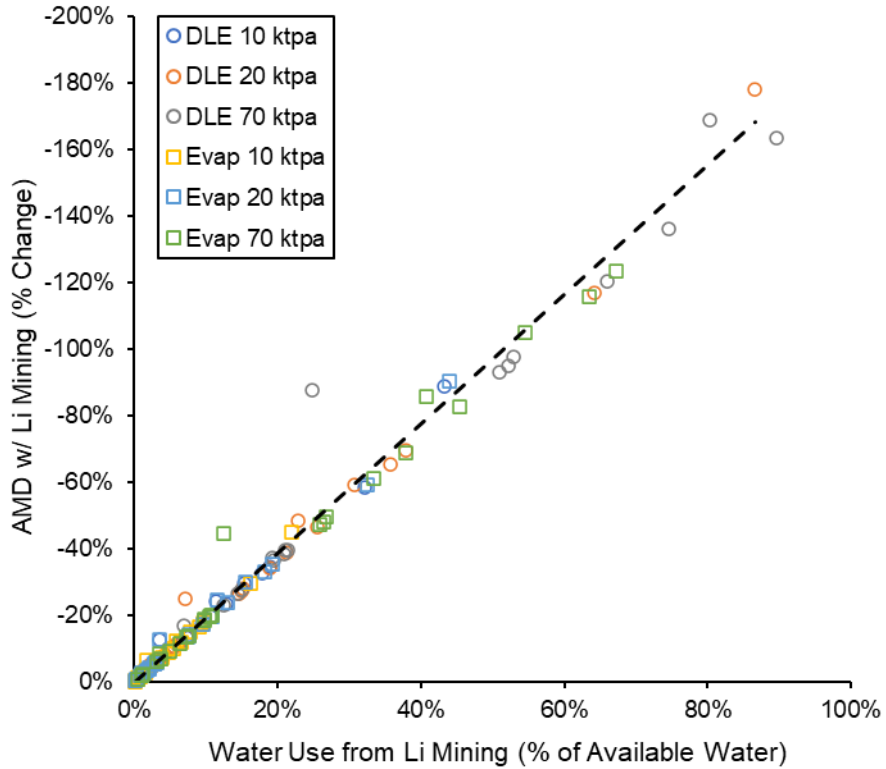


Figure S4: The percentage of total available water (groundwater recharge plus streamflow) being consumed from Li mining vs. percent change in AMD when incorporating freshwater use from Li mining (Figure 5). Circle symbols represent the AMD reduction when using direct lithium extraction (DLE), while the square symbols represent the use of evaporative technology. The plot shows that a 40% reduction in available water from Corkran et al. (2024) is comparable to an ~80% reduction in AMD in Figure 5. The dotted black line represents a linear regression for all data.

Table S1: Mean absolute error (MAE) and root-mean-square error (RMSE) for all 13 precipitation products assessed. This includes the 10 products with historical records back to 1980 and the 3 products that were only assessed using the 1996-2016 stations shown in Figure 1 because of limited historical records. This table also includes the MAE and RMSE when only using the stations with greater than a 95% complete record.

	Precipitation Product	MAE (mm/year)	MAE (%)	RMSE (mm/year)	MRSE (%)
All Stations (n=26)	TerraClimate	58	13%	89	20%
	MSWEP V2.2	88	20%	105	24%
	CFSv2	111	25%	168	38%
	CRU TS 4.07	135	31%	162	37%
	ERA-5	222	51%	244	56%
	CHIRPS	238	54%	295	67%
	WFDEI	267	61%	395	90%
	PERSIANN-CDR	276	63%	322	74%
	GPCC	286	65%	437	100%
	GPCP	289	66%	360	82%
Stations >95% Record (n=19)	TerraClimate	48	11%	70	16%
	MSWEP V2.2	74	17%	82	19%
	CFSv2	118	27%	184	42%
	CRU TS 4.07	122	28%	151	34%
	WFDEI	216	49%	351	80%
	CHIRPS	220	50%	285	65%
	ERA-5	223	51%	248	57%
	GPCC	231	53%	390	89%
	GPCP	242	55%	313	72%
	PERSIANN-CDR	269	61%	321	73%
1996-2016 Stations (n=7)	TerraClimate (1996-2016)	31	7%	56	13%
	GPM IMERG (2001-2016)	42	10%	52	12%
	TRMM (1998-2016)	68	16%	75	17%
	CMORPH CDR (1998-2016)	266	61%	305	70%

Table S2: Basin attributes and results from availability minus demand calculations. All units are in mm per year unless otherwise labeled. Each column includes an average with the minimum and maximum associated values in parentheses. The minimum and maximum values for precipitation represent one standard deviation above and below the mean.

Basin ID	Basin Name	Watershed Area (km ²)	Basin Floor Area (km ²)	Basin Floor Elevation (m asl)	Precipitation	Groundwater Recharge	Streamflow	Available Water	Human Water Consumption	Environmental Water Requirements	Availability minus Demand (AMD)
1	Salir de Uyuni	47,219	12,320	3,654	114 (81.6 - 146.4)	3.2 (2 - 5.2)	9.1 (6.1 - 13.9)	12.2 (8.1 - 19.1)	0.4	5.5	6.3 (2.3 - 13.2)
2	Laguna de Guayalayoc	6,994	375	3,401	205.4 (165.4 - 245.4)	11.7 (4.3 - 26.4)	21.1 (14.2 - 32.3)	32.8 (18.5 - 58.7)	0.2	14.7	17.8 (3.6 - 43.8)
3	Salir de Pujsa	633	34	4,507	78.8 (51.4 - 106.3)	1.8 (1.2 - 2.9)	8 (5.4 - 12.3)	9.8 (6.6 - 15.1)	0.7	4.4	4.7 (1.4 - 10)
4	Salir de Jama	2,069	28	4,075	87.7 (67.3 - 108.2)	2.2 (1.3 - 3.8)	9.3 (6.2 - 14.2)	11.4 (7.5 - 18)	0.2	5.1	6.1 (2.2 - 12.6)
5	Laguna Lejia	197	3	4,325	66.3 (42.6 - 90)	1.3 (0.9 - 2)	7 (4.7 - 10.7)	8.3 (5.7 - 12.7)	0.5	3.7	4.1 (1.4 - 8.5)
6	Salir de Alacama	17,395	2,171	2,300	37.4 (19.6 - 55.2)	0.5 (0.5 - 0.5)	3.6 (2.4 - 5.5)	4.1 (2.9 - 6)	0.6	1.8	1.7 (0.5 - 3.6)
7	Salir de Olanos-Cauchari	5,685	590	3,898	109.7 (89.1 - 130.3)	3.1 (1.8 - 5.8)	10.6 (7.1 - 16.2)	13.7 (8.9 - 22)	0.0	6.2	7.5 (2.7 - 15.8)
8	Salinas Grandes	10,509	472	3,407	142.6 (118.2 - 166.9)	5.4 (2.6 - 11.1)	14.5 (9.8 - 22.3)	20 (12.3 - 33.4)	0.1	9.0	10.9 (3.3 - 24.3)
9	Laguna Tuyajto	249	6	4,033	70.7 (50.8 - 90.6)	1.5 (1 - 2.3)	7.4 (5 - 11.4)	8.9 (6 - 13.7)	0.0	4.0	4.9 (2 - 9.7)
10	Salir del Rincon	2,763	423	3,720	81.5 (64.3 - 98.7)	1.8 (1.2 - 2.8)	7.5 (5 - 11.5)	9.2 (6.2 - 14.3)	0.1	4.2	5 (2 - 10)
11	Salir de Pular	728	34	3,571	52.9 (36.1 - 69.8)	0.9 (0.7 - 1.2)	5.5 (3.7 - 8.4)	6.3 (4.4 - 9.6)	0.2	2.9	3.3 (1.3 - 6.5)
12	Salir de Pastos Grandes	1,627	48	3,772	115.9 (97.8 - 134)	3.7 (1.9 - 7.1)	12.1 (8.1 - 18.6)	15.8 (10.1 - 25.7)	0.4	7.1	8.2 (2.5 - 18.2)
13	Salir de Pochitos	2,538	434	3,657	84.1 (69.5 - 98.6)	1.8 (1.3 - 2.9)	7.5 (5.1 - 11.5)	9.4 (6.3 - 14.5)	0.1	4.2	5.1 (2.1 - 10.2)
14	Salir de Punta Negra	4,188	244	2,950	20 (6.62 - 33.4)	0.2 (0.1 - 0.3)	2 (1.4 - 3.1)	2.2 (1.5 - 3.4)	0.0	1.0	1.2 (0.5 - 2.4)
15	Salir de Pozuelos	385	71	3,756	92.6 (77.5 - 107.7)	2.2 (1.4 - 3.6)	8.2 (5.5 - 12.5)	10.3 (6.9 - 16.1)	0.0	4.6	5.7 (2.2 - 11.5)
16	Salir de Arizaro	6,723	2,277	3,469	53.3 (38.1 - 68.5)	1 (0.9 - 1.1)	4 (2.7 - 6.1)	4.9 (3.6 - 7.1)	0.0	2.2	2.7 (1.3 - 4.9)
17	Salir de Lullillaco	1,231	124	3,754	40.4 (25.3 - 55.4)	0.6 (0.5 - 0.6)	4 (2.7 - 6.1)	4.5 (3.2 - 6.7)	0.0	2.0	2.5 (1.1 - 4.6)
18	Salir de Ratones-Centenario	1,664	110	3,809	107.7 (90.9 - 124.5)	3.1 (1.7 - 5.9)	10.9 (7.3 - 16.6)	14 (9 - 22.5)	0.1	6.3	7.6 (2.6 - 16.1)
19	Salir Toillar	1,024	44	3,610	76.7 (63.4 - 90)	1.7 (1.1 - 2.7)	7.9 (5.3 - 12.1)	9.5 (6.4 - 14.8)	0.0	4.3	5.2 (2.1 - 10.5)
20	Salir de Rio Grande	1,378	162	3,655	44.1 (30.6 - 57.5)	0.6 (0.6 - 0.7)	4.2 (2.8 - 6.4)	4.8 (3.4 - 7.2)	0.0	2.2	2.7 (1.2 - 5)
21	Salir de Diablillos	497	44	4,030	116.6 (98.5 - 134.8)	3.6 (2 - 6.9)	11.5 (7.8 - 17.7)	15.2 (9.7 - 24.6)	0.0	6.8	8.3 (2.9 - 17.8)
22	Laguna Caro	342	15	3,990	86.1 (70.2 - 101.9)	2.1 (1.3 - 3.6)	8.9 (6 - 13.6)	10.9 (7.3 - 17.1)	0.0	4.9	6 (2.3 - 12.2)
23	Salir del Hombre Muerto	3,881	483	3,964	105.3 (87.4 - 123.2)	3 (1.7 - 5.5)	10.2 (6.8 - 15.6)	13.2 (8.6 - 21)	0.2	5.9	7.1 (2.5 - 14.9)
24	Salir de Antofalla	5,860	689	3,323	59.0 (45.6 - 72.5)	1 (0.8 - 1.5)	5.8 (3.9 - 8.8)	6.8 (4.7 - 10.3)	0.0	3.1	3.7 (1.6 - 7.2)
25	Salir de Carachi Pampa	6,442	109	3,004	81.5 (64.8 - 98.1)	1.9 (1.3 - 3.2)	8.6 (5.8 - 13.2)	10.6 (7.1 - 16.4)	0.0	4.8	5.8 (2.3 - 11.6)
26	Salir de Incabasi	1,148	44	3,262	67.2 (49.6 - 84.8)	1.3 (0.9 - 2)	7 (4.7 - 10.7)	8.3 (5.6 - 12.7)	0.0	3.7	4.6 (1.9 - 9)
27	Salir de Maricunga	2,417	147	3,752	67.7 (27.7 - 107.6)	1.4 (1 - 2.1)	6.9 (4.7 - 10.6)	8.3 (5.6 - 12.7)	2.2	3.7	2.3 (-0.3 - 6.7)
28	Tres Quebradas	2,793	114	4,082	95.1 (46.7 - 143.5)	2.5 (1.5 - 4.5)	9.8 (6.6 - 15.1)	12.4 (8.1 - 19.5)	0.1	5.6	6.7 (2.4 - 13.9)

Table S3: Availability minus demand after incorporating freshwater use from lithium mining (AMD_{Li}). The columns include AMD_{Li} values when utilizing two lithium processing technologies (the only production-scale direct lithium extraction method and evaporative technology) and producing 10, 20, and 70 kilo-tonnes per annum (ktpa) LCE. The average and range (shown in parentheses) represent AMD_{Li} when using the range of AMD values presented Table S2. All units are in mm per year.

Basin ID	Basin Name	Current Full-Scale Direct Lithium Extraction			Evaporative Technology		
		AMD _{Li} 10 ktpa	AMD _{Li} 20 ktpa	AMD _{Li} 70 ktpa	AMD _{Li} 10 ktpa	AMD _{Li} 20 ktpa	AMD _{Li} 70 ktpa
1	Salár de Uyuni	6.3 (2.2 - 13.2)	6.3 (2.2 - 13.2)	6.2 (2.2 - 13.1)	6.3 (2.3 - 13.2)	6.3 (2.2 - 13.2)	6.3 (2.2 - 13.2)
2	Laguna de Guayatayoc	17.7 (3.5 - 43.7)	17.6 (3.4 - 43.6)	17.1 (2.9 - 43.1)	17.8 (3.5 - 43.7)	17.7 (3.5 - 43.7)	17.5 (3.2 - 43.4)
3	Salár de Pujasa	3.5 (0.3 - 8.9)	2.4 (-0.8 - 7.8)	-3.2 (-6.4 - 2.1)	4.1 (0.9 - 9.4)	3.5 (0.3 - 8.9)	0.7 (-2.5 - 6)
4	Salár de Jama	5.7 (1.8 - 12.3)	5.4 (1.5 - 11.9)	3.7 (-0.2 - 10.2)	5.9 (2 - 12.4)	5.7 (1.8 - 12.3)	4.8 (1 - 11.4)
5	Laguna Lejía	0.4 (-2.2 - 4.9)	-3.2 (-5.8 - 1.2)	-21.2 (-23.9 - -16.8)	2.2 (-0.4 - 6.6)	0.4 (-2.3 - 4.8)	-8.7 (-11.4 - -4.3)
6	Salár de Atacama	1.6 (0.4 - 3.6)	1.6 (0.4 - 3.6)	1.4 (0.2 - 3.3)	1.7 (0.5 - 3.6)	1.6 (0.4 - 3.6)	1.5 (0.3 - 3.5)
7	Salár de Olaroz-Cauchari	7.4 (2.6 - 15.7)	7.3 (2.4 - 15.5)	6.6 (1.8 - 14.9)	7.4 (2.6 - 15.7)	7.4 (2.6 - 15.7)	7.1 (2.3 - 15.4)
8	Salinas Grandes	10.8 (3.2 - 24.2)	10.8 (3.1 - 24.2)	10.4 (2.8 - 23.8)	10.9 (3.2 - 24.3)	10.8 (3.2 - 24.2)	10.6 (3 - 24.1)
9	Laguna Tuyajito	2 (-0.8 - 6.8)	-0.8 (-3.7 - 4)	-15.1 (-18 - -10.3)	3.4 (0.6 - 8.2)	2 (-0.9 - 6.8)	-5.2 (-8.1 - -0.5)
10	Salár del Rincon	4.7 (1.7 - 9.8)	4.4 (1.4 - 9.5)	3.2 (0.2 - 8.2)	4.8 (1.8 - 9.9)	4.7 (1.7 - 9.8)	4 (1 - 9.1)
11	Salár de Pular	2.3 (0.4 - 5.5)	1.4 (-0.6 - 4.6)	-3.5 (-5.5 - -0.3)	2.8 (0.8 - 6)	2.3 (0.3 - 5.5)	-0.2 (-2.1 - 3.1)
12	Salár de Pastos Grandes	7.8 (2.1 - 17.7)	7.4 (1.7 - 17.3)	5.2 (-0.5 - 15.1)	8 (2.3 - 17.9)	7.8 (2.1 - 17.7)	6.7 (1 - 16.6)
13	Salár de Pochitos	4.8 (1.8 - 9.9)	4.5 (1.5 - 9.7)	3.2 (0.1 - 8.3)	5 (1.9 - 10.1)	4.8 (1.8 - 9.9)	4.1 (1.1 - 9.2)
14	Salár de Punta Negra	1 (0.3 - 2.2)	0.9 (0.1 - 2)	0 (-0.7 - 1.2)	1.1 (0.4 - 2.3)	1 (0.3 - 2.2)	0.6 (-0.1 - 1.8)
15	Salár de Pozuelos	3.8 (0.4 - 9.6)	2 (-1.4 - 7.8)	-7.3 (-10.7 - -1.5)	4.7 (1.3 - 10.5)	3.8 (0.4 - 9.6)	-0.9 (-4.3 - 4.9)
16	Salár de Arizaro	2.6 (1.2 - 4.8)	2.5 (1.1 - 4.7)	2 (0.6 - 4.2)	2.6 (1.3 - 4.8)	2.6 (1.2 - 4.8)	2.3 (1 - 4.5)
17	Salár de Lullillaco	1.9 (0.5 - 4.1)	1.3 (0 - 3.5)	-1.6 (-2.9 - 0.6)	2.2 (0.8 - 4.3)	1.9 (0.5 - 4)	0.4 (-0.9 - 2.6)
18	Salár de Ratones-Centenario	7.1 (2.2 - 15.7)	6.7 (1.8 - 15.2)	4.6 (-0.4 - 13.1)	7.3 (2.4 - 15.9)	7.1 (2.2 - 15.6)	6.1 (1.1 - 14.6)
19	Salár Toillar	4.5 (1.4 - 9.8)	3.8 (0.7 - 9.1)	0.4 (-2.8 - 5.6)	4.9 (1.7 - 10.1)	4.5 (1.4 - 9.8)	2.8 (-0.4 - 8)
20	Salár de Río Grande	2.1 (0.7 - 4.5)	1.6 (0.2 - 3.9)	-1 (-2.4 - 1.4)	2.4 (0.9 - 4.7)	2.1 (0.7 - 4.5)	0.8 (-0.6 - 3.1)
21	Salár de Diablillos	6.9 (1.5 - 16.3)	5.5 (0 - 14.9)	-1.7 (-7.1 - 7.7)	7.6 (2.2 - 17)	6.9 (1.4 - 16.3)	3.3 (-2.2 - 12.7)
22	Laguna Caro	3.9 (0.2 - 10.1)	1.8 (-1.9 - 8)	-8.5 (-12.2 - -2.4)	4.9 (1.2 - 11.1)	3.9 (0.2 - 10.1)	-1.4 (-5.1 - 4.8)
23	Salár del Hombre Muerto	6.9 (2.3 - 14.8)	6.7 (2.1 - 14.6)	5.8 (1.2 - 13.7)	7 (2.4 - 14.8)	6.9 (2.3 - 14.8)	6.4 (1.8 - 14.3)
24	Salár de Antofalía	3.6 (1.4 - 7.1)	3.5 (1.3 - 7)	2.9 (0.7 - 6.3)	3.6 (1.5 - 7.1)	3.6 (1.4 - 7.1)	3.3 (1.1 - 6.8)
25	Salár de Carachi Pampa	5.7 (2.2 - 11.5)	5.6 (2.1 - 11.4)	5 (1.5 - 10.9)	5.7 (2.2 - 11.6)	5.7 (2.2 - 11.5)	5.4 (1.9 - 11.2)
26	Salár de Incahuasi	3.9 (1.3 - 8.3)	3.3 (0.7 - 7.7)	0.2 (-2.4 - 4.6)	4.2 (1.6 - 8.7)	3.9 (1.3 - 8.3)	2.4 (-0.3 - 6.8)
27	Salár de Maricunga	2.1 (-0.6 - 6.4)	1.8 (-0.9 - 6.1)	0.3 (-2.4 - 4.7)	2.2 (-0.5 - 6.6)	2.1 (-0.6 - 6.4)	1.3 (-1.4 - 5.7)
28	Tres Quebradas	6.5 (2.2 - 13.6)	6.2 (1.9 - 13.4)	4.9 (0.7 - 12.1)	6.6 (2.3 - 13.8)	6.5 (2.2 - 13.6)	5.8 (1.5 - 13)